

The nature of $X(3872)$ from high-multiplicity pp collisions

Angelo Esposito,¹ Elena G. Ferreira,² Alessandro Pilloni,^{3,4} Antonio D. Polosa,⁵ and Carlos A. Salgado²

¹*Theoretical Particle Physics Laboratory (LPTP),*

Institute of Physics, EPFL, 1015 Lausanne, Switzerland

²*Instituto Galego de Física de Altas Enerxías – IGFAE,*

Universidade de Santiago de Compostela, E-15782 Santiago de Compostela, Galicia-Spain

³*European Centre for Theoretical Studies in Nuclear Physics and related Areas*

(ECT) and Fondazione Bruno Kessler, Villazzano (Trento), I-38123, Italy*

⁴*INFN Sezione di Genova, Genova, I-16146, Italy*

⁵*Dipartimento di Fisica and INFN, Sapienza Università di Roma, Piazzale Aldo Moro 2, I-00185 Roma, Italy*

The structure of exotic resonances that do not trivially fit the usual quark model expectations has been a matter of strong scientific debate during the last two decades. An excellent way to measure the size of these states is to observe how much they are affected when immersed in QCD matter. Recently, LHCb has measured the relative abundance of the exotic $X(3872)$ over the ordinary $\psi(2S)$. Built on several decades of phenomenological understanding of quarkonia production in hot and dense QCD matter, we employ the comover interaction model to study the yield of the $X(3872)$. To confirm the reliability of the model in large multiplicity pp collisions, we describe the larger suppression of excited over ground Υ states, as well as the enhancement of deuterons over protons, for which coalescence is implemented. With this at hand, we show that the size of the $X(3872)$ is only slightly larger than that of the $\psi(2S)$, that is, it corresponds to a typical hadronic state. This finding clearly supports the $X(3872)$ being a tetraquark state and strongly disfavors the molecular interpretation, that would need a much larger size.

The last two decades witnessed a remarkable progress in heavy meson spectroscopy. Several new states, called XYZ, have been observed in the quarkonium sector, close to open flavor thresholds. Their properties are not well described by the conventional quark model/NRQCD, whence they are expected to have an exotic structure. In particular, the $X(3872)$, observed as an unexpected peak in the $J/\psi \pi^+ \pi^-$ invariant mass, was the first of the series [1]. Its mass is almost exactly at the $\bar{D}^0 D^{*0}$ threshold, and is remarkably narrow [2, 3].¹ The pion pair is dominated by the ρ meson, thus showing a substantial amount of isospin violation, unexpected if the X were an ordinary charmonium. The structure of this state has been subject of an intense debate [4–6].

Since the simple $c\bar{c}$ description cannot account for the observed features of $X(3872)$, more valence quarks are needed. They can be aggregated by color forces in a new kind of hadron, a compact tetraquark, or by nuclear forces in a bound state, a molecule, of two mesons. Since the $X(3872)$ mass is so close to the $\bar{D}^0 D^{*0}$ threshold, it could be an example of a hadron molecule with an extremely small binding energy and a size of the order of 10 fm [5, 7], or more. Alternatively, it might be interpreted as a compact, ~ 1 fm, tetraquark state [4, 8–10].

Recently, the LHCb collaboration has presented the production rates of promptly produced $X(3872)$ relative to the $\psi(2S)$, as a function of final state particle multiplicity [11]. This ratio is found to decrease with increasing multiplicity, evoking the expected fragile molecule behavior of $X(3872)$. However, a similar effect has been known for decades to affect the production of ordinary quarkonia

in proton-nucleus collisions. There is an ample consensus for this to be due to final state breakup interactions of the quarkonia with comoving particles [12].

The ALICE collaboration has recently published an analysis, analogous to the LHCb one, for deuteron production in proton-proton collisions [13]. The number of deuterons produced increases with multiplicity, further contradicting the naïve expectations for the $X(3872)$. The idea that interactions with comovers could favor the coalescence of a hadron molecule was originally proposed in [14, 15] for proton-proton, and in [16–18] for nucleus-nucleus collisions.

In this work we show, for the first time, how the comover model of [12, 23] correctly reproduces also the bottomonium production in proton-proton collisions, for multiplicities higher than the mean value. The suppression increases with increasing number of comovers, similarly to the proton-nucleus case. We then apply the same method to the $X(3872)$. The results for a compact tetraquark are in agreement with the LHCb data. The same mechanism applied to a hadron molecule turns into a suppression too strong to explain the data.

However, data on deuteron show an important role of recombination for molecular states, which is irrelevant for compact ones. Therefore, we revisit the comover model to implement the coalescence mechanism proposed in [14]. While this reproduces deuteron data, it fails with the $X(3872)$. Our results are therefore consistent with a compact tetraquark interpretation of the $X(3872)$, and a destruction cross section comparable to that of other compact states.

¹ Charge conjugation is understood throughout the paper.

	$E_{\mathcal{Q}}^{\text{thr}}$	$r_{\mathcal{Q}}$	$\sigma_{\mathcal{Q}}^{\text{geo}}$	$\langle v\sigma \rangle_{\mathcal{Q}}$
$\psi(2S)$	50 MeV	0.45 fm	6.36 mb	5.15 ± 0.84 mb
$X(3872)$ tetraquark	116 keV	0.65 fm	13.3 mb	11.61 ± 1.69 mb
$X(3872)$ molecule	116 keV	6.6 fm	1368 mb	1197 ± 171 mb

TABLE I. Fixed values used in our parametrisation of the comover cross sections and the resulting values. The average over the comover distribution $\langle v\sigma \rangle_{\mathcal{Q}}$ and its uncertainties are described in the text. The threshold energy is computed with respect to the closest OZI-favored mode, given the available comover energy. This is $D^0\bar{D}^0$ - D^+D^- for the charmonium. For a tetraquark $X(3872)$, the closest available is \bar{D}^0D^{*0} [19], the OZI-favored mode $\Lambda_c^+\Lambda_c^-$ [20–22] being kinematically forbidden at the typical comover’s energy. The average for this binding energy is 44 ± 116 keV [2, 3]. In our calculations, we use as binding energy the 1σ error. The radius of the tetraquark is taken from [10, 19].

I. THE COMOVER INTERACTION MODEL

To include final state interactions, we follow the comover interaction model (CIM) [12, 23]. Within this framework, quarkonia are broken by collisions with comovers—*i.e.* final state particles with similar rapidities. The density of quarkonium $\rho_{\mathcal{Q}}$, at a given transverse coordinate s and rapidity y , for a collision of impact parameter b , evolves in time with

$$\tau \frac{d\rho_{\mathcal{Q}}}{d\tau}(b, s, y) = -\langle v\sigma \rangle_{\mathcal{Q}} \rho_c(b, s, y) \rho_{\mathcal{Q}}(b, s, y), \quad (1)$$

where $\langle v\sigma \rangle_{\mathcal{Q}}$ is the cross section of quarkonium dissociation, averaged over the momentum distributions of the comoving particles, whose transverse density is ρ_c at initial time τ_i . The above equation neglects recombination effects which, for a compact object, are irrelevant due to the paucity of heavy quarks produced in the pp environment considered. Integrating Eq. (1) from τ_i to τ_f ,

$$\rho_{\mathcal{Q}} \propto \exp \left[-\langle v\sigma \rangle_{\mathcal{Q}} \rho_c(b, s, y) \ln \left(\frac{\rho_c(b, s, y)}{\rho_{pp}(y)} \right) \right], \quad (2)$$

where the argument of the logarithm comes from τ_f/τ_i converted in ratios of densities. The interaction stops at τ_f when the densities have diluted down to ρ_{pp} , the value of pp density at the same energy and rapidity.

The comover density is directly connected to the charged particle multiplicity N_{ch} by $\rho_c = \frac{3}{2}N_{\text{ch}}/\sigma$. The factor $3/2$ accounts for the neutral comovers, while σ corresponds to a pp cross section. From the eikonal-Glauber model [24], which successfully reproduces charged multiplicities in proton and nuclear collisions, we have estimated the pp non-diffractive cross section to be 63 mb at 7 TeV and 70 mb at 13 TeV, while the inelastic values are slightly higher (see also [25]). The two lead to no appreciable difference in the final results.

As can be seen from Eq. (1), the abundance of a quarkonium \mathcal{Q} is driven by its interaction cross section with the comovers $\langle v\sigma \rangle_{\mathcal{Q}}$. While in nucleus-nucleus collisions at lower energies the latter has been fitted from data (independently state by state), it can be generically related to

the quarkonium geometrical cross section and its threshold energy by [12]

$$\langle v\sigma \rangle_{\mathcal{Q}} = \sigma_{\mathcal{Q}}^{\text{geo}} \left\langle \left(1 - \frac{E_{\mathcal{Q}}^{\text{thr}}}{E_c} \right)^n \right\rangle. \quad (3)$$

Here $\sigma_{\mathcal{Q}}^{\text{geo}} \equiv \pi r_{\mathcal{Q}}^2$, with $r_{\mathcal{Q}}$ being the quarkonium radius. Moreover, $E_{\mathcal{Q}}^{\text{thr}}$ is the energy of the quarkonium relative to the closest OZI-favored threshold, and E_c the energy of the comovers in the quarkonium center-of-mass frame. The average is computed over a Bose-Einstein distribution,

$$\mathcal{P}(E_c) \propto \frac{1}{e^{E_c/T_{\text{eff}}} - 1} \theta(E_c - E_{\mathcal{Q}}^{\text{thr}}). \quad (4)$$

Both n and T_{eff} are purely phenomenological parameters. Attempts to compute n using the multipole expansion in perturbative QCD at leading order would suggest that $n \simeq 4$ for pion comovers, by making the strong assumption that the scattering is initiated by the gluons inside these pions [26–28]. More realistic hadronic models suggest a smaller value [29, 30]. For this reason, we will consider n varying from 0.5 to 2.

We recall two features of the comover approach. First, larger particles are more affected by dissociation, due to larger interaction cross sections. As a consequence, excited states are more suppressed than the ground states. Second, the suppression increases with comover densities, which is proportional to particle multiplicities: it increases with centrality in nucleus-nucleus collisions, and it will be stronger in the nucleus direction for proton-nucleus collisions.

A fit on the relative yields of excited over ground state Υ s data at LHC energies gives an effective temperature T_{eff} in the range of 200 to 300 MeV for our assumed range of n [12]. These values are quite independent of the mass of the comovers, whether gluonic or hadronic. The resulting cross sections for the Υ s, ranking from less than 0.1 mb for the ground state up to some mb for the $3S$ and $3P$ states, successfully reproduce data of proton-nucleus collisions [12]. For proton-proton, the yields have been measured by CMS at 2.76 TeV, as a function of the number of charged particles with $p_T > 400$ MeV, reconstructed

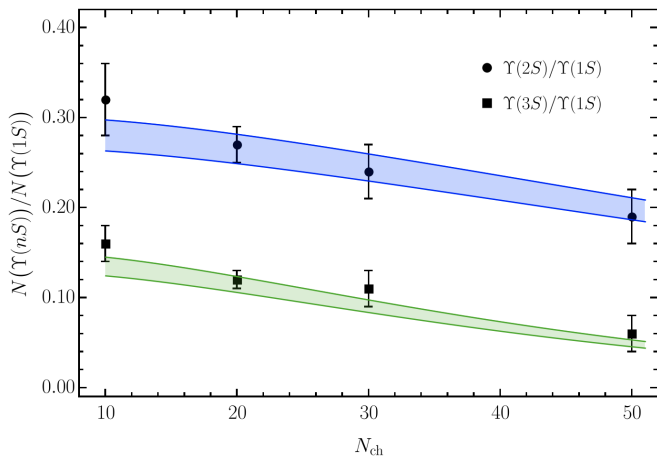


FIG. 1. Relative yields of excited-to-ground state Υ as a function of event multiplicity for pp collisions at 2.76 TeV in the central region, as measured by CMS [31]. The bands correspond to the propagation of the uncertainties of the cross sections that contribute via the feed down. Our results are normalised to the experimental value corresponding to the mean multiplicity.

in the tracker at $|\eta| < 2.4$ [31]. Data are shown together with our results in Figure 1, confirming the validity of the model. Errors are estimated taking into account the ones of the cross sections of the six states that contribute via feed down. The global normalisation corresponds to the experimental value at the mean multiplicity.

We extend our calculation to charmonia by applying Eq. (3) for the cross sections. Although the value of n , which encodes non-perturbative effects, could in principle be different from the bottomonium one, we get cross section values in the ballpark of those obtained by directly fitting the charmonium data [32], confirming that a unified description is possible.

II. THE $X(3872)$ IN THE CIM MODEL

The relative production rates of prompt $X(3872)$ over $\psi(2S)$ have been measured by LHCb in pp collisions at 8 TeV, in the forward pseudorapidity region, $2 < \eta < 5$ [11]. These are given as a function of the number of charged particle tracks reconstructed in the VELO detector. This ratio is found to decrease with increasing multiplicity.

As mentioned above, the suppression of the state is driven by its interaction cross section with the comovers, estimated in Eq. (3). Since the latter is proportional to the geometric cross section, extremely different results are expected for a compact state such a tetraquark, or a large loosely-bound molecule. These are reported in Table I for the two cases. We calculate the ratio $N(X(3872))/N(\psi(2S))$ versus N_{ch} . We normalize our results to the first bin. Figure 2 shows our results for the two $X(3872)$ hypotheses.

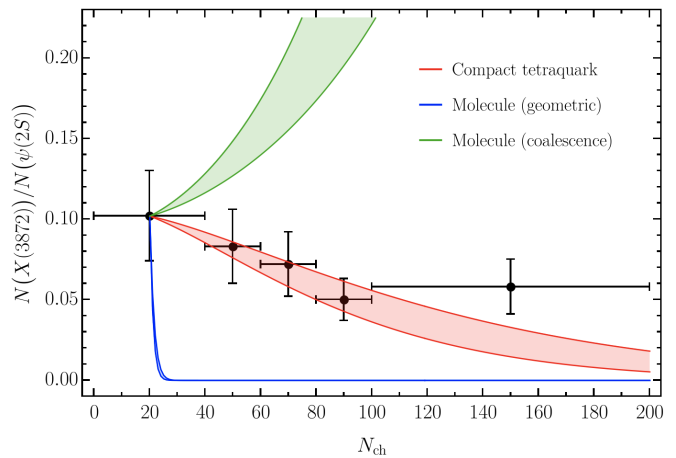


FIG. 2. Relative yield of $X(3872)$ vs $\psi(2S)$ as a function of event multiplicity for pp collisions at 8 TeV and forward pseudorapidity, as measured by LHCb [11]. The assumption of a tetraquark of size 1.3 fm reproduces well the experimental data. Extending the CIM to a molecular state via its geometrical cross section predicts a very sharp suppression. The coalescence picture predicts a qualitatively different behavior, still in clear contradiction with data.

For a tetraquark of size 1.3 fm, the CIM predicts a decrease of about 20% in the ratio when going from the first to the second multiplicity bin. Incidentally, this decrease is similar to that of the Υ states, see Figure 1. On the other hand, in case of a large $X(3872)$ molecule, the assumption of a geometrical cross section leads to a suppression so strong that no $X(3872)$ would survive past the second bin in clear contradiction with the data.

III. COALESCENCE OF HADRON MOLECULES

The implementation of comover interactions discussed above disregards recombination. While surely negligible for compact states, recombination is needed to explain deuteron data: the deuteron yield increases with increasing multiplicity of the final state [13]. Were a molecular X to behave like that, it would be in striking contrast with the data in [11]. The common description of the destruction and recombination of molecules is in terms of coalescence. In this picture the constituents are bound/free depending on whether their relative momentum is smaller/larger than some coalescence momentum Λ . The creation or destruction of a molecule can hence be induced by the interaction with comovers, an idea put forth in a number of papers [14, 16–18]. In [14] it has been proposed that the driving process is given by the scattering $\pi hh \rightleftharpoons \pi m$, where hh are free molecular constituents, m the molecule itself and π the comover.

Accounting for these processes, the evolution of the molecules with time can be described by the extension of

Eq. (1) derived in Appendix A following [33], *i.e.*

$$\tau \frac{dN_m}{d\tau} = \langle v\sigma \rangle_m \rho_c N_{12} - \left(\langle v\sigma \rangle_m + \langle v\sigma \rangle_{hh} \right) \rho_c N_m, \quad (5)$$

where N_m and N_{12} are the number of molecules and the total number of constituent pairs respectively (taken to be constant in time), whereas $\langle v\sigma \rangle_m$ and $\langle v\sigma \rangle_{hh}$ are the average cross sections for the creation and destruction of a molecule due to the interaction with a comover. The averages are taken over the initial distributions for the free constituents, molecules and comovers. We compute the momentum distribution of the molecule perturbatively around the free stream solution [34]. Eq. (5) has a relatively simple solution for the number of molecules as a function of the event multiplicity, N_{ch} :

$$\frac{N_m}{N_{12}} = \frac{\langle v\sigma \rangle_m}{\langle v\sigma \rangle_{hh} + \langle v\sigma \rangle_m} + \left(\frac{N_m^0}{N_{12}} - \frac{\langle v\sigma \rangle_m}{\langle v\sigma \rangle_{hh} + \langle v\sigma \rangle_m} \right) \times \exp \left[-(\langle v\sigma \rangle_{hh} + \langle v\sigma \rangle_m) \rho_c \ln(\rho_c / \rho_c^{pp}) \right], \quad (6)$$

were N_m^0 is the number of molecules generated by hadronization, before any further interaction with comovers. The dependence on multiplicity comes from the comovers spatial density. Note that for $\langle v\sigma \rangle_m = 0$ the result above reduces to Eq. (2), upon volume integration.

We test the validity of this idea on data. For deuteron we consider a coalescence momentum in the range $\Lambda = 50$ – 250 MeV [35]. The momentum distributions for the free constituents and for the comovers² are taken from `Pythia8` [36], while those for deuteron are taken directly from data [13]. The comover-constituent interaction is given by an effective coupling obtained by averaging the πN elastic cross section for kinetic energies up to 300 MeV (see [37] and Appendix B). With this information at hand one can compute the average cross sections for creation and destruction of a deuteron (see Appendix C), obtaining $\langle v\sigma \rangle_m \simeq (\Lambda/150 \text{ MeV})^3 \times 0.51 \text{ mb}$ and $\langle v\sigma \rangle_{hh} \simeq 4.34 \text{ mb}$. We also estimate the number of initial deuterons with `Pythia8`, by counting how many proton-neutron pairs have relative momentum initially below Λ . We find $N_m^0/N_{12} = O(10^{-4})$, which can be neglected. In this way the dependence of the number of deuterons on multiplicity is fixed, up to an overall factor, which we fit to data. We also set ρ_c^{pp} such that the curve starts at $N_{\text{ch}} = 1$, as in data.

In Figure 3 we compare our results to the ALICE data. The good match confirms the validity of the coalescence approach, and of the idea proposed in [14], especially the relevance of the comovers to the enhancement of the production of hadron molecules.

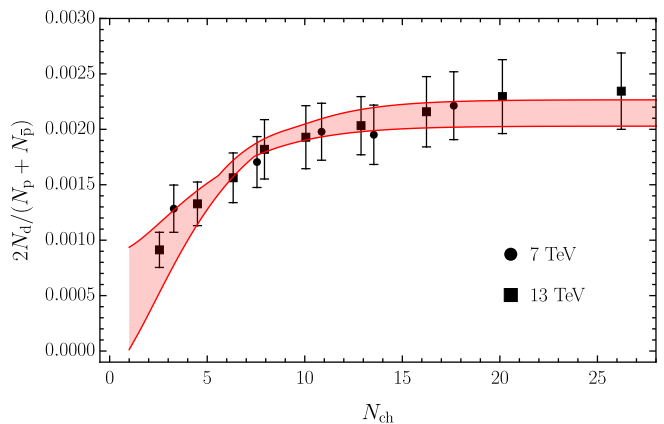


FIG. 3. Number of deuterons over number of protons at 7 and 13 TeV of center-of-mass energy as a function of multiplicity, as reported in [13]. The solid line is our result (6), the uncertainty being determined by varying the coalescence momentum Λ between 50 and 250 MeV [35].

IV. THE $X(3872)$ IN THE COALESCENCE MODEL

We can now apply the same procedure to the $X(3872)$. The momentum distributions for the comovers and for the free $\bar{D}^0 D^{*0}$ pairs are again taken from `Pythia8`, while those for the $X(3872)$ are obtained from a NRQCD calculation [38], which reproduces well the prompt production data at high p_{\perp} [39]. The coalescence momentum for the $X(3872)$ is taken to be $\Lambda = 50$ MeV [14, 40]. The effective coupling is obtained averaging over $\pi D^{(*)} \rightarrow \pi D^{(*)}$ cross section up to 300 MeV. The matrix element is built to reproduce the scattering lengths from [41] and to include D^* exchanges [42] (more details in Appendix B). The corresponding average cross sections are $\langle v\sigma \rangle_m \simeq 3.1 \times 10^{-5} \text{ mb}$ and $\langle v\sigma \rangle_{hh} \simeq 0.50 \text{ mb}$, the first one being much smaller with respect to the deuteron one, given the tiny binding energy. Note that the destruction cross section is in good agreement with what obtained in [17] with different methods and for different inelastic processes.

As for the initial number of $X(3872)$ produced by hadronization alone, N_m^0 , there is still no consensus. On the one hand, a purely molecular interpretation requires for this number to be very small because of the difficulty in producing the constituents with such a small relative momentum [40], as for the deuteron, albeit some controversies on the role of final state interactions [38, 42]. On the other hand, it has been suggested that the production of the $X(3872)$ could be dominated by the short distance physics, likely associated to a charmonium component of its wave function [43]. Were this to be true, the prompt production cross section could be significantly enhanced. Here we adopt an agnostic viewpoint and let the initial number of molecules vary from $N_m^0/N_{12} = 0$ (the estimate with `Pythia8` being 10^{-6}) to $N_m^0/N_{12} = 1$. We consider this to be the main source of uncertainty in

² In our simulations we define as a comover any long-lived particle whose momentum lies in a cone $\Delta R < 0.4$ from one of the constituents (the other constituent is clearly excluded).

our calculation. Either way, the molecular nature of the $X(3872)$ must be manifest when propagating throughout the comovers for distances of $O(1 \text{ fm})$.

Our results are reported in Figure 2, and are again at odds with data, for both the scenarios. The number of $X(3872)$ normalized to $\psi(2S)$ always grows. Indeed, if the initial number $X(3872)$ is close to zero, recombination (albeit small) increases the number of molecules. If, instead, the state is copiously produced by hadronization, the overall number of molecules decreases with multiplicity. However, the decrease is milder than that of $\psi(2S)$, hence the shape of the curve.

V. CONCLUSIONS

The production of $X(3872)$ at high transverse momenta in low multiplicity pp collisions challenges the molecular interpretation [18, 40], to the extent that it is necessary to assume its hadronization proceeds through a compact $c\bar{c}$ core. In [14] it was indeed shown that not even the interaction with comoving particles was able to account for the large number of $X(3872)$, if this compact component is not considered. However, the recent presentation of high-multiplicity data from the LHCb and ALICE collaborations [11, 13], encourages to reconsider the role of comovers.

In this paper we redesigned the molecule-comover interaction model, treating multiple scattering with kinetic theory. This works remarkably well at explaining the deuteron production reported by ALICE [13]. Were a sizeable molecular component to appear in the $X(3872)$ wave function, the same approach should describe its relative yield with respect to $\psi(2S)$ [11]. However, the predicted yield always grows and cannot match the decreasing slope observed by LHCb. The only way to reconcile the results from the coalescence model with experiment is to make the averaged $X(3872)$ molecular destruction cross section, $\langle v\sigma \rangle_{hh}$, about twenty times larger, in sharp contradiction with several agreeing determinations of the interaction couplings of pion comovers with D, D^* mesons and with the findings in [17], for example.

The LHCb results are analyzed also with the Comover Interaction Model (CIM) [12, 23], which is well known to describe the quarkonia yields in high multiplicity final states. The yields are determined by the geometrical cross section, and eventually by the size of the states. For the first time, we apply the CIM to pp collisions, and match the relative yields of Υ s with the ones reported by CMS [31]. These yields decrease with multiplicity, contradicting the statement that such a behavior requires a molecular interpretation, as suggested for the $X(3872)$. Conversely, it is perfectly compatible with a compact tetraquark of hadronic size, as we show here. In the CIM, the molecular $X(3872)$ is way more fragile against collisions with comovers, because of its large size. This leaves no space to a loosely-bound $X(3872)$ in the over-densely populated stream of comovers. To reconcile this

result with experiment one needs a geometrical cross section two orders of magnitude smaller, falling in the region attributed to compact structures.

We look with interest also to PbPb data [44], which seem to present novelties with respect to pp . It would be useful to have them binned in centrality, to allow a comparison with the deuteron data presented by ALICE [45]. Discussions on tetraquarks and molecules in PbPb collisions can be found in [46].

In conclusion, as soon as the loosely-bound molecule description is made concrete, both approaches discussed in this paper fail at reproducing the $X(3872)$ data by large deviations that cannot be adjusted by a judicious tuning of parameters. In our view, the LHCb data on the $X(3872)$ display the same features characterizing compact states like the Υ s.

ACKNOWLEDGMENTS

E.G.F. thanks Frédéric Fleuret, Jean-Philippe Lansberg and Sarah Porteboeuf, who encouraged the applicability of the comover interaction to proton-proton collisions, and for fruitful discussions during the development of this work. Also, we thank Matt Durham, Benjamin Audurier, Oscar Boente, and especially Luciano Maiani for valuable discussions. We are also grateful to Alexis Pompili for pointing the CMS and LHCb results presented at Quark Matter 2020 to us, and to Giuseppe Mandaglio for valuable insights on the experimental analysis by the ALICE collaboration. A.E. is supported by the Swiss National Science Foundation under contract 200020-169696 and through the National Center of Competence in Research SwissMAP. E.G.F. and C.A.S. are supported by Ministerio de Ciencia e Innovación of Spain under project FPA2017-83814-P; Unidad de Excelencia María de Maetzu under project MDM-2016-0692; and Xunta de Galicia (Consellería de Educación) and FEDER. C.A.S. is supported by ERC-2018-ADG-835105 YoctoLHC.

Appendix A: Boltzmann equation for hadron molecules and comovers

In this derivation, we will follow [33]. In particular, we will use the standard noncovariant form of the Boltzmann equation, and all the quantities discussed below are meant to be defined in the lab frame. We discuss the creation and destruction of hadron molecules as due to elastic scattering of a comover with one of the constituents [14, 18]. For example, for the deuteron we restrict to processes like $\pi pn \rightleftharpoons \pi d$.

Consider two hadrons, ‘1’ and ‘2’, with positions and momenta $(\mathbf{x}_1, \mathbf{q}_1)$ and $(\mathbf{x}_2, \mathbf{q}_2)$. We adopt the coalescence picture, *i.e.* that the two hadrons bind if their relative momentum is smaller than some threshold, $|\mathbf{q}_1 - \mathbf{q}_2| < \Lambda$. The phase-space density for these two

hadrons, $n_{12}(\mathbf{x}_1, \mathbf{x}_2, \mathbf{q}_1, \mathbf{q}_2, \tau)$, is such that

$$\begin{aligned} N_m(\tau) &= \int d^3x_1 d^3x_2 \int_{\mathcal{R}_\Lambda} \frac{d^3q_1}{(2\pi)^3} \frac{d^3q_2}{(2\pi)^3} n_{12}(\mathbf{x}_i, \mathbf{q}_i, \tau), \\ N_{hh}(\tau) &= \int d^3x_1 d^3x_2 \int_{\bar{\mathcal{R}}_\Lambda} \frac{d^3q_1}{(2\pi)^3} \frac{d^3q_2}{(2\pi)^3} n_{12}(\mathbf{x}_i, \mathbf{q}_i, \tau), \\ N_{12} &= \int d^3x_1 d^3x_2 \int \frac{d^3q_1}{(2\pi)^3} \frac{d^3q_2}{(2\pi)^3} n_{12}(\mathbf{x}_i, \mathbf{q}_i, \tau), \end{aligned} \quad (\text{A1})$$

where \mathcal{R}_Λ is the domain where $|\mathbf{q}_1 - \mathbf{q}_2| < \Lambda$, and $\bar{\mathcal{R}}_\Lambda$ its complement. N_m , N_{hh} and N_{12} are respectively the number of molecules, free pairs and total pairs. Clearly $N_{12} = N_m + N_{hh}$, and it is assumed to be constant in time, hence neglecting creation/annihilation of the constituents themselves. In the lab frame, the variable τ can be taken simply as the time.

We assume that the spatial and momentum distributions factorize as

$$n_{12} \simeq \begin{cases} \rho_m(\mathbf{x}_i, \tau) f_m(\mathbf{q}_i, \tau) & \text{for } |\mathbf{q}_1 - \mathbf{q}_2| < \Lambda \\ \rho_{hh}(\mathbf{x}_i, \tau) f_{hh}(\mathbf{q}_i, \tau) & \text{for } |\mathbf{q}_1 - \mathbf{q}_2| \geq \Lambda \end{cases}, \quad (\text{A2})$$

where both f_m and f_{hh} are normalized to unity when integrated over their momentum domain.

Collisions with comovers change the momenta of the constituents, and consequently modify their distribution. Choosing the z -axis to be in the beam direction, the Boltzmann equation reduces to [33]:

$$\begin{aligned} \frac{\partial n_{12}}{\partial \tau} - \frac{q_{1z}}{\tau} \frac{\partial n_{12}}{\partial q_{1z}} - \frac{q_{2z}}{\tau} \frac{\partial n_{12}}{\partial q_{2z}} &= -L(\mathbf{x}_i, \mathbf{q}_i, \tau) \\ &+ G(\mathbf{x}_i, \mathbf{q}_i, \tau), \end{aligned} \quad (\text{A3})$$

where the loss and gain terms are, respectively

$$\begin{aligned} L &= \int \frac{d^3q_3}{(2\pi)^3} \frac{d^3q'_2}{(2\pi)^3} \frac{d^3q'_3}{(2\pi)^3} W(\mathbf{q}_2, \mathbf{q}_3; \mathbf{q}'_2, \mathbf{q}'_3) \delta_P \times \\ &\times n_{12}(\mathbf{x}_1, \mathbf{x}_2, \mathbf{q}_1, \mathbf{q}_2, \tau) n_c(\mathbf{x}_2, \mathbf{q}_3, \tau), \end{aligned} \quad (\text{A4a})$$

$$\begin{aligned} G &= \int \frac{d^3q_3}{(2\pi)^3} \frac{d^3q'_2}{(2\pi)^3} \frac{d^3q'_3}{(2\pi)^3} W(\mathbf{q}_2, \mathbf{q}_3; \mathbf{q}'_2, \mathbf{q}'_3) \delta_P \times \\ &\times n_{12}(\mathbf{x}_1, \mathbf{x}_2, \mathbf{q}_1, \mathbf{q}'_2, \tau) n_c(\mathbf{x}_2, \mathbf{q}'_3, \tau). \end{aligned} \quad (\text{A4b})$$

Here W is the nonrelativistic matrix element for the $q_2 + q_3 \rightleftharpoons q'_2 + q'_3$ process, and $\delta_P \equiv (2\pi)^4 \delta^{(4)}(q_2 + q_3 - q'_2 - q'_3)$ enforces conservation of energy and momentum. We have assumed that comovers interact with constituents ‘1’ and ‘2’ equally. Without loss of generality, we have restricted the interaction to the constituent ‘2’, so that the position of the comover must be \mathbf{x}_2 . The interaction with ‘1’ is taken into account later, by a factor of 2 in the cross sections. Moreover, n_c is the phase-space distribution of comovers, which again we factorize as $n_c(\mathbf{x}, \mathbf{q}, \tau) \simeq \rho_c(\mathbf{x}, \tau) f_c(\mathbf{q}, \tau)$.

To study the evolution of the density of molecules, we now integrate Eq. (A3) over \mathbf{q}_1 and \mathbf{q}_2 in \mathcal{R}_Λ . We also assume that the momentum distribution of the molecule follows the free-stream (collisionless) distribution [34]. After that, the left hand side of Eq. (A3) simply returns $\partial \rho_m(\mathbf{x}_i, \tau) / \partial \tau$. The loss term instead gives

$$\int_{\mathcal{R}_\Lambda} \frac{d^3q_1}{(2\pi)^3} \frac{d^3q_2}{(2\pi)^3} L \simeq \rho_m(\mathbf{x}_i, \tau) \rho_c(\mathbf{x}_2, \tau) \langle v\sigma \rangle_{hh}, \quad (\text{A5})$$

where the average cross section for the destruction of a molecule is defined as

$$\begin{aligned} \langle v\sigma \rangle_{hh} &\equiv \int_{\mathcal{R}_\Lambda} \frac{d^3q_1}{(2\pi)^3} \frac{d^3q_2}{(2\pi)^3} \int \frac{d^3q_3}{(2\pi)^3} \frac{d^3q'_2}{(2\pi)^3} \frac{d^3q'_3}{(2\pi)^3} \times \\ &\times W(\mathbf{q}_2, \mathbf{q}_3; \mathbf{q}'_2, \mathbf{q}'_3) \delta_P f_m(\mathbf{q}_1, \mathbf{q}_2, \tau) f_c(\mathbf{q}_3, \tau). \end{aligned} \quad (\text{A6})$$

The gain term instead requires a bit more care. Imposing momentum conservation, its integral over \mathcal{R}_Λ gives

$$\begin{aligned} \int_{\mathcal{R}_\Lambda} \frac{d^3q_1}{(2\pi)^3} \frac{d^3q_2}{(2\pi)^3} G &= \int_{\mathcal{R}_\Lambda} \frac{d^3q_1}{(2\pi)^3} \frac{d^3q_2}{(2\pi)^3} \int \frac{d^3q_3}{(2\pi)^3} \frac{d^3q'_2}{(2\pi)^3} \frac{d^3q'_3}{(2\pi)^3} W(\mathbf{q}_2, \mathbf{q}_3; \mathbf{q}'_2, \mathbf{q}'_3) \delta_P \times \\ &\times n_{12}(\mathbf{x}_1, \mathbf{x}_2, \mathbf{q}_1, \mathbf{q}_2 + \mathbf{q}_3 - \mathbf{q}'_3, \tau) n_c(\mathbf{x}_2, \mathbf{q}'_3, \tau). \end{aligned} \quad (\text{A7})$$

The relative momentum appearing in the distribution is then $(\mathbf{q}_1 - \mathbf{q}_2) + (\mathbf{q}'_3 - \mathbf{q}_3)$. Now, by construction $|\mathbf{q}_1 - \mathbf{q}_2| < \Lambda$, while the comovers distribution in the lab frame is dominated by momenta $|\mathbf{q}'_3| \gg \Lambda$. This

means that, barring small integration regions, for most configurations $|(\mathbf{q}_1 - \mathbf{q}_2) + (\mathbf{q}'_3 - \mathbf{q}_3)| \gtrsim \Lambda$, and we can

use Eq. (A2) and write

$$\int_{\mathcal{R}_\Lambda} \frac{d^3 q_1}{(2\pi)^3} \frac{d^3 q_2}{(2\pi)^3} G \simeq \rho_{hh}(\mathbf{x}_i, \tau) \rho_c(\mathbf{x}_2, \tau) \langle v\sigma \rangle_m, \quad (\text{A8})$$

with average cross section for the creation of a molecule given by

$$\langle v\sigma \rangle_m \equiv \int_{\mathcal{R}_\Lambda} \frac{d^3 q_1}{(2\pi)^3} \frac{d^3 q_2}{(2\pi)^3} \int \frac{d^3 q_3}{(2\pi)^3} \frac{d^3 q'_2}{(2\pi)^3} \frac{d^3 q'_3}{(2\pi)^3} \times (\text{A9}) \\ \times W(\mathbf{q}_2, \mathbf{q}_3; \mathbf{q}'_2, \mathbf{q}'_3) \delta_P f_{hh}(\mathbf{q}_1, \mathbf{q}'_2, \tau) f_c(\mathbf{q}'_3, \tau).$$

The Boltzmann equation then reads

$$\frac{\partial \rho_m(\mathbf{x}_i, \tau)}{\partial \tau} \simeq \rho_{hh}(\mathbf{x}_i, \tau) \rho_c(\mathbf{x}_2, \tau) \langle v\sigma \rangle_m \quad (\text{A10}) \\ - \rho_m(\mathbf{x}_i, \tau) \rho_c(\mathbf{x}_2, \tau) \langle v\sigma \rangle_{hh}.$$

Finally, if the density of comovers is roughly homogeneous, we can integrate over \mathbf{x}_1 and \mathbf{x}_2 as well. The final evolution equation then reads

$$\frac{\partial N_m(\tau)}{\partial \tau} \simeq \rho_c(\tau) (N_{hh}(\tau) \langle v\sigma \rangle_m - N_m(\tau) \langle v\sigma \rangle_{hh}) \\ = \rho_c(\tau) N_{12} \langle v\sigma \rangle_m \quad (\text{A11}) \\ - \rho_c(\tau) N_m(\tau) (\langle v\sigma \rangle_m + \langle v\sigma \rangle_{hh}).$$

In the last line we used the fact that $N_{12} = N_m + N_{hh}$. In the free-stream approximation, the spatial density of comovers evolves with time as $\rho_c(\tau) = \rho_c/\tau$, with ρ_c the *transverse* density at formation time τ_i . With this approximation, the Boltzmann equation can be solved exactly, and gives

$$\frac{N_m(\tau_f)}{N_{12}} = \frac{\langle v\sigma \rangle_m}{\langle v\sigma \rangle_{hh} + \langle v\sigma \rangle_m} \\ + \left(\frac{N_m^0}{N_{12}} - \frac{\langle v\sigma \rangle_m}{\langle v\sigma \rangle_{hh} + \langle v\sigma \rangle_m} \right) \times \quad (\text{A12}) \\ \times \exp \left[-(\langle v\sigma \rangle_{hh} + \langle v\sigma \rangle_m) \rho_c \ln(\tau_f/\tau_i) \right],$$

with τ_f the time at which the comovers become dilute enough to stop interacting with the pairs. Considering the scaling of $\rho_c(\tau)$ with time one can take $\tau_f/\tau_i = \rho_c/\rho_c^{pp}$, where ρ_c^{pp} is the density of comovers for a pp collision with no interactions.

Appendix B: Effective couplings for comover-constituent interaction

To simplify the computation we effectively describe the comover-constituent scattering with a constant relativistic matrix element, $\mathcal{M}_{\pi h \rightarrow \pi h} = g^2$. As our notation suggests, we estimate this effective coupling by assuming that comovers are pions only, which indeed dominate.

For the case of the deuteron, the effective coupling is obtained by matching the total elastic pion-nucleon

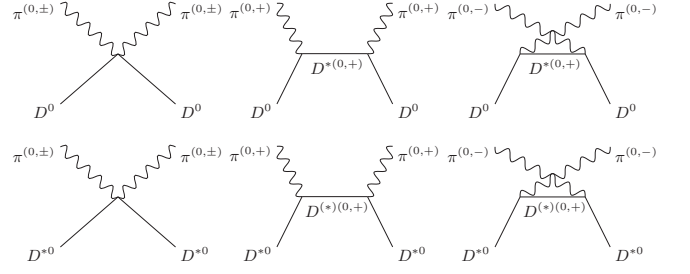


FIG. 4. Feynman diagrams for the $\pi D^{(*)} \rightarrow \pi D^{(*)}$ elastic scatterings considered to extract the effective coupling g .

cross section from PDG [3], averaged in the $[0, 300 \text{ MeV}]$ kinetic energy range for the comover. Therefore reaching the peak of the intermediate Δ resonance. One gets $g^2/(4\pi) \simeq 10$, which is not far from the threshold value $g^2/(4\pi) \simeq 13.5$ [37].

For the $X(3872)$ no data are available for the $\pi D^{(*)} \rightarrow \pi D^{(*)}$ scattering. To obtain the coupling we then consider the following Lagrangian for the interaction between pions and heavy mesons

$$\mathcal{L}_{\text{int}} = -\frac{y}{f_\pi} \text{tr} (\bar{H}_a H_b \gamma_\mu \gamma_5) \partial^\mu \mathcal{M}_{ba} \quad (\text{B1}) \\ + \frac{\lambda}{4M} \text{tr} (\bar{H}_a H_a) \mathcal{M}_{ab} \mathcal{M}_{ba}.$$

Here a, b are isospin indices, the traces are taken over Dirac matrices and M is the mass of the heavy mesons. Moreover, H_a is the HQET heavy meson multiplet and \mathcal{M}_{ab} is the pion matrix. The trilinear coupling is given by $y \simeq 0.8$ [42]. We take the propagator of the D^* to be

$$\frac{-i}{p^2 - m_D^2 + im_D \Gamma_{D^*}} \left(g^{\mu\nu} - \frac{p^\mu p^\nu}{p^2} \right), \quad (\text{B2})$$

the real part of the pole being at the mass of the D to avoid collinear divergences in the u -channel (note that the D and D^* are indeed degenerate at leading order in HQET). Moreover, we choose the projector to be exactly transverse (rather than only on-shell) to make sure that the contribution from the off-shell D^* propagation vanishes at threshold. This way, the only contribution to the scattering length is given by the quartic coupling, which is found to be $\lambda \simeq 25$, by matching with lattice calculation of the πD scattering length [41].

Given the above vertices, the effective coupling g is again obtained matching the total elastic πD cross section averaged over the kinetic energy of the comover in the range 0–300 MeV. The processes we considered are reported in Figure 4. The result is $g^2/(4\pi) \simeq 5.07$.

Appendix C: Creation and destruction average cross sections

We describe how to extract the value of the average cross sections (A6) and (A9). The calculation is conceptually straightforward but rather tedious. We will spare

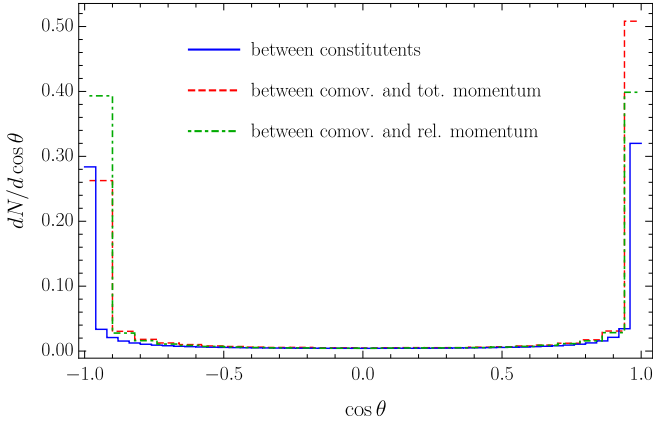


FIG. 5. Distributions obtained from `Pythia8` for the relative polar angle between the deuteron constituents (blue, solid), the comovers and the total momentum of the molecule (red, dashed) and the comovers and relative momentum of the constituents (green, dot-dashed). Everything is computed in the lab frame. Results are equivalent for the $X(3872)$.

most of it to the reader, and only highlight the main points.

First of all, we always work in the approximation of roughly massless comovers, $m_c \simeq 0$, and of loosely bound molecule, *i.e.* $\Lambda \ll |\mathbf{q}_i|$. In particular, the latter implies that the momenta of the constituents are approximately equal to each other and to half the momentum of the molecule itself.

To study the momentum distributions with `Pythia8`, we generate 750k pp events at $\sqrt{s} = 7$ TeV for deuteron, and 2.5G pp events at 8 TeV for the $X(3872)$, with full-QCD $2 \rightarrow 2$ matrix elements and a cut on the partonic transverse momentum, $\hat{p}_\perp > 2$ GeV. Long-lived particles are prevented from decaying. We select all the events that have at least one constituent pair in the final state and, when more than one pair per event is available, all the combinations are considered. By comovers, we mean all those particles whose momentum lies in a cone $\Delta R < 0.4$ from one of the constituents (the other constituent is clearly excluded).

In the lab frame, most particles have large momentum component along the beam axis. The polar angles between the constituents' momenta, between the comovers' and the molecule's momentum, as well as between the comovers' and the constituents' relative momentum can thus be approximated by $\cos \theta \simeq \pm 1$, see Figure 5.

After this, the two integrals can be reduced to

$$\langle v\sigma \rangle_m \simeq \frac{\Lambda^3 g^4}{384\pi} \int dP dk \frac{k^2 P^2 f_{hh}(P, k)}{\sqrt{M^2 + \frac{(P+k)^2}{4}} \sqrt{M^2 + \frac{(P-k)^2}{4}}} \sum_{\pm} f_c \left(\frac{k \pm \Delta E}{2} \right) \left| \frac{k \pm \Delta E}{k \mp \Delta E} \right|, \quad (\text{C1a})$$

$$\langle v\sigma \rangle_{hh} \simeq \frac{g^4}{32\pi} \int dP \frac{P^2 f_m(P)}{\sqrt{M^2 + \frac{P^2}{4}}} \int_{P/2}^{\infty} dq'_2 \frac{q'_2}{\sqrt{M^2 + q_2'^2}} \int_{q_3^{\min}}^{\infty} dq_3 \frac{q_3 f_c(q_3)}{\left(\frac{P}{2} + q_3\right)} \theta \left(\sqrt{M^2 + \frac{P^2}{4}} + q_3 \geq \sqrt{M^2 + q_2'^2} \right). \quad (\text{C1b})$$

Here g is the comover-constituent coupling defined in Appendix B, P and k the total and relative momenta of the hadron pair and M the mass of the constituents, which we take to be approximately equal. Moreover, $\Delta E \equiv \sqrt{M^2 + \frac{(P+k)^2}{4}} - \sqrt{M^2 + \frac{(P-k)^2}{4}}$, while the minimum value of the momentum q_3 is

$$q_3^{\min} \equiv \frac{\sqrt{4M^2 + P^2} \sqrt{M^2 + q_2'^2} - 2M^2 - q_2' P}{2q_2' + \sqrt{4M^2 + P^2} - P - 2\sqrt{M^2 + q_2'^2}}. \quad (\text{C2})$$

The distributions extracted from `Pythia8` are reported in Figure 6 for both the proton-neutron and the $\bar{D}^0 D^{*0}$ pairs. They are well described by the following functional

forms:

$$f_c(q_3) \propto \frac{e^{-\alpha_2 q_3} + \alpha_1 e^{-\alpha_3 q_3}}{q_3^2}, \quad (\text{C3a})$$

$$f_{hh}(P, k) \propto \frac{\ln(1 + \beta_2 P)^{\beta_1} \ln(1 + \gamma_2 k)^{\gamma_1}}{P^3 (1 + \beta_2 P)^{\beta_3} k^3 (1 + \gamma_2 k)^{\gamma_3}}, \quad (\text{C3b})$$

with best fit values given in Table II. The overall constant is fixed by normalization. The distribution of the total momentum of the molecule can instead be obtained from the experimental distributions in transverse momentum and rapidity. In particular

$$\begin{aligned} P^2 f_m(P) &= \int dP_\perp dy F_m(P_\perp, y) \delta \left(P - \sqrt{P_\perp^2 + (4M^2 + P_\perp^2) \sinh^2 y} \right) \\ &= \int_0^P dP_\perp \frac{2P F_m(P_\perp, \bar{y}(P_\perp))}{\sqrt{4M^2 + P^2} \sqrt{P^2 - P_\perp^2}} \theta(\bar{y}(P_\perp) \leq Y), \end{aligned} \quad (\text{C4})$$

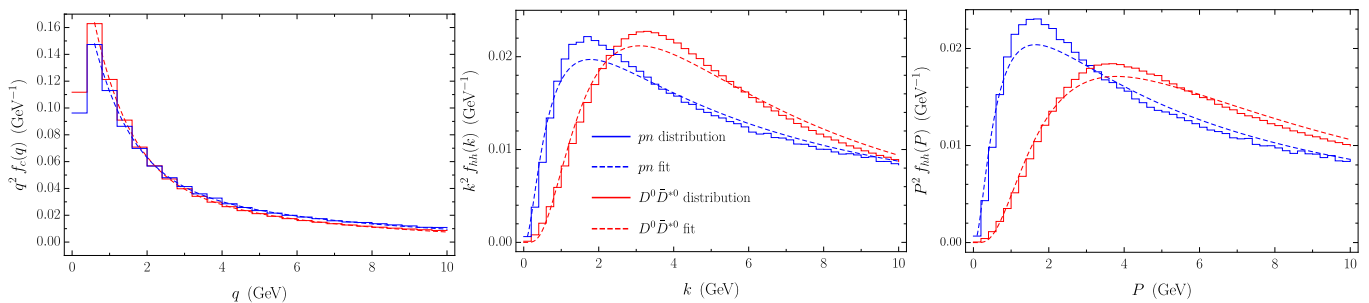


FIG. 6. Distributions obtained from `Pythia8` for the momentum of the comovers (left), the relative momentum of the hadron pair (center) and the total momentum of the pair (right) together with the best fit curves (dashed lines). Again, everything is computed in the lab frame, at $\sqrt{s} = 7$ TeV for the pn pairs and $\sqrt{s} = 8$ TeV for the $\bar{D}^0 D^{*0}$ ones.

	α_1	α_2 (GeV) $^{-1}$	α_3 (GeV) $^{-1}$	β_1	β_2 (GeV) $^{-1}$	β_3	γ_1	γ_2 (GeV) $^{-1}$	γ_3
pn pairs	3.49	0.17	0.97	4.12	3.43	0	3.99	2.90	0
$\bar{D}^0 D^{*0}$ pairs	4.04	0.20	1.03	7.85	2.09	2.46	7.33	1.67	2.84

TABLE II. Best fit parameters for the distribution in Eqs. (C3) as obtained from `Pythia8`.

with $F_m(P_\perp, y)$ the experimental distribution, assumed even under $y \rightarrow -y$, Y the experimental cut in rapidity, and $\sinh \bar{y} \equiv \sqrt{(P^2 - P_\perp^2)/(4M^2 + P_\perp^2)}$.

With these distributions at hand one can compute the average cross sections in Eqs. (C1). For the deuteron we take $M = 938$ MeV and a coalescence momentum in the range $\Lambda = 50$ –250 MeV [35]. The effective cou-

pling g is discussed in Appendix B. The distribution in rapidity is approximately uniform, while the one in transverse momentum is well fitted by a Lévy-Tsallis function [13]. We obtain $\langle v\sigma \rangle_m \simeq (\Lambda/150 \text{ MeV})^3 \times 0.51$ mb and $\langle v\sigma \rangle_{hh} \simeq 4.34$ mb. For the $X(3872)$ we instead take $M = \frac{1}{2}(m_D + m_{D^*}) = 1936$ MeV, and $\Lambda = 50$ MeV [14, 40]. The result is $\langle v\sigma \rangle_m \simeq 3.1 \times 10^{-5}$ mb and $\langle v\sigma \rangle_{hh} \simeq 0.50$ mb.

-
- [1] S.-K. Choi *et al.* (Belle), *Phys.Rev.Lett.* **91**, 262001 (2003), [arXiv:hep-ex/0309032](#).
- [2] R. Aaij *et al.* (LHCb), [arXiv:2005.13419 \[hep-ex\]](#) (2020); [arXiv:2005.13422 \[hep-ex\]](#) (2020).
- [3] M. Tanabashi *et al.* (Particle Data Group), *Phys.Rev.* **D98**, 030001 (2018).
- [4] A. Esposito, A. Pilloni, and A. D. Polosa, *Phys.Rept.* **668**, 1 (2017), [arXiv:1611.07920 \[hep-ph\]](#).
- [5] F.-K. Guo, C. Hanhart, U.-G. Meißner, Q. Wang, Q. Zhao, and B.-S. Zou, *Rev.Mod.Phys.* **90**, 015004 (2018), [arXiv:1705.00141 \[hep-ph\]](#).
- [6] S. L. Olsen, T. Skwarnicki, and D. Zieminska, *Rev.Mod.Phys.* **90**, 015003 (2018), [arXiv:1708.04012 \[hep-ph\]](#); N. Brambilla, S. Eidelman, C. Hanhart, A. Nefediev, C.-P. Shen, C. E. Thomas, A. Vairo, and C.-Z. Yuan, [arXiv:1907.07583 \[hep-ex\]](#) (2019).
- [7] E. Braaten and M. Kusunoki, *Phys.Rev.* **D69**, 074005 (2004), [arXiv:hep-ph/0311147 \[hep-ph\]](#); F. E. Close and P. R. Page, *Phys.Lett.* **B578**, 119 (2004), [arXiv:hep-ph/0309253 \[hep-ph\]](#); N. A. Tornqvist, *Phys.Lett.* **B590**, 209 (2004), this report supersedes the unpublished reminder [hep-ph/0308277](#), [arXiv:hep-ph/0402237 \[hep-ph\]](#); E. S. Swanson, *Phys.Rept.* **429**, 243 (2006), [arXiv:hep-ph/0601110 \[hep-ph\]](#).
- [8] L. Maiani, F. Piccinini, A. D. Polosa, and V. Riquer, *Phys.Rev.* **D71**, 014028 (2005), [arXiv:hep-ph/0412098 \[hep-ph\]](#).
- [9] S. J. Brodsky, D. S. Hwang, and R. F. Lebed, *Phys.Rev.Lett.* **113**, 112001 (2014), [arXiv:1406.7281 \[hep-ph\]](#).
- [10] A. Esposito and A. D. Polosa, *Eur.Phys.J.* **C78**, 782 (2018), [arXiv:1807.06040 \[hep-ph\]](#).
- [11] LHCb Collaboration (LHCb) (2019), [LHCb-CONF-2019-005](#).
- [12] E. Ferreira, *Phys.Lett.* **B749**, 98 (2015), [arXiv:1411.0549 \[hep-ph\]](#); E. G. Ferreira and J.-P. Lansberg, *JHEP* **10**, 094, [Erratum: *JHEP* 03, 063 (2019)], [arXiv:1804.04474 \[hep-ph\]](#).
- [13] S. Acharya *et al.* (ALICE), *Phys.Lett.* **B794**, 50 (2019), [arXiv:1902.09290 \[nucl-ex\]](#); [arXiv:2003.03184 \[nucl-ex\]](#) (2020).
- [14] A. Esposito, F. Piccinini, A. Pilloni, and A. Polosa, *J.Mod.Phys.* **4**, 1569 (2013), [arXiv:1305.0527 \[hep-ph\]](#); A. Guerrieri, F. Piccinini, A. Pilloni, and A. Polosa, *Phys.Rev.* **D90**, 034003 (2014), [arXiv:1405.7929 \[hep-ph\]](#).
- [15] A. Esposito, A. L. Guerrieri, F. Piccinini, A. Pilloni, and A. D. Polosa, *Int.J.Mod.Phys.* **A30**, 1530002 (2014), [arXiv:1411.5997 \[hep-ph\]](#).

- [16] M. Gyulassy, I. Vitev, X.-N. Wang, and B.-W. Zhang, [arXiv:nucl-th/0302077 \[nucl-th\]](#) (2003).
- [17] S. Cho *et al.* (ExHIC), *Phys.Rev.Lett.* **106**, 212001 (2011), [arXiv:1011.0852 \[nucl-th\]](#); S. Cho and S. H. Lee, *Phys.Rev.* **C88**, 054901 (2013), [arXiv:1302.6381 \[nucl-th\]](#).
- [18] A. Esposito, A. L. Guerrieri, L. Maiani, F. Piccinini, A. Pilloni, A. D. Polosa, and V. Riquer, *Phys.Rev.* **D92**, 034028 (2015), [arXiv:1508.00295 \[hep-ph\]](#).
- [19] L. Maiani, A. D. Polosa, and V. Riquer, *Phys.Lett.* **B778**, 247 (2018), [arXiv:1712.05296 \[hep-ph\]](#).
- [20] L. Montanet, G. Rossi, and G. Veneziano, *Phys.Rept.* **63**, 149 (1980).
- [21] G. Rossi and G. Veneziano, *JHEP* **06**, 041, [arXiv:1603.05830 \[hep-th\]](#).
- [22] G. Cotugno, R. Faccini, A. Polosa, and C. Sabelli, *Phys.Rev.Lett.* **104**, 132005 (2010), [arXiv:0911.2178 \[hep-ph\]](#).
- [23] A. Capella, E. Ferreira, and A. Kaidalov, *Phys.Rev.Lett.* **85**, 2080 (2000), [arXiv:hep-ph/0002300](#); A. Capella, L. Bravina, E. Ferreira, A. Kaidalov, K. Tywoniuk, and E. Zabrodin, *Eur.Phys.J.* **C58**, 437 (2008), [arXiv:0712.4331 \[hep-ph\]](#); E. Ferreira, *Phys.Lett.* **B731**, 57 (2014), [arXiv:1210.3209 \[hep-ph\]](#).
- [24] A. Capella and E. Ferreira, *Eur.Phys.J.* **C72**, 1936 (2012), [arXiv:1110.6839 \[hep-ph\]](#).
- [25] J. Welti, *Inelastic, non-diffractive and diffractive proton-proton cross-section measurements at the LHC*, Ph.D. thesis, U. Helsinki (2017).
- [26] G. Bhanot and M. E. Peskin, *Nucl.Phys.* **B156**, 391 (1979).
- [27] D. Kharzeev and H. Satz, *Phys.Lett.* **334**, B155 (1994), [hep-ph/9405414](#).
- [28] H. Satz, *J.Phys.* **G32**, R25 (2006), [arXiv:hep-ph/0512217](#).
- [29] K. Martins, D. Blaschke, and E. Quack, *Phys.Rev.* **C51**, 2723 (1995), [arXiv:hep-ph/9411302 \[hep-ph\]](#).
- [30] R. Rapp, D. Blaschke, and P. Crochet, *Prog.Part.Nucl.Phys.* **65**, 209 (2010), [arXiv:0807.2470 \[hep-ph\]](#).
- [31] S. Chatrchyan *et al.* (CMS), *JHEP* **04**, 103, [arXiv:1312.6300 \[nucl-ex\]](#).
- [32] N. Armesto and A. Capella, *Phys.Lett.* **B430**, 23 (1998), [arXiv:hep-ph/9705275](#).
- [33] G. Baym, *Phys.Lett.* **B138**, 18 (1984).
- [34] H. Heiselberg and A.-M. Levy, *Phys.Rev.* **C59**, 2716 (1999), [arXiv:nucl-th/9812034](#); H. Heiselberg and X.-N. Wang, *Phys.Rev.* **C53**, 1892 (1996), [arXiv:hep-ph/9504244](#); H. Heiselberg and R. Mattiello, *Phys.Rev.* **C60**, 044902 (1999).
- [35] A. Ibarra and S. Wild, *JCAP* **02**, 021, [arXiv:1209.5539 \[hep-ph\]](#); L. Dal and A. Raklev, *Phys.Rev.* **D89**, 103504 (2014), [arXiv:1402.6259 \[hep-ph\]](#); T. Aramaki *et al.*, *Phys.Rept.* **618**, 1 (2016), [arXiv:1505.07785 \[hep-ph\]](#).
- [36] T. Sjöstrand, S. Ask, J. R. Christiansen, R. Corke, N. Desai, P. Ilten, S. Mrenna, S. Prestel, C. O. Rasmussen, and P. Z. Skands, *Comput.Phys.Commun.* **191**, 159 (2015), [arXiv:1410.3012 \[hep-ph\]](#).
- [37] E. Matsinos, [arXiv:1901.01204 \[nucl-th\]](#) (2019).
- [38] P. Artoisenet and E. Braaten, *Phys.Rev.* **D81**, 114018 (2010), [arXiv:0911.2016 \[hep-ph\]](#).
- [39] S. Chatrchyan *et al.* (CMS), *JHEP* **1304**, 154, [arXiv:1302.3968 \[hep-ex\]](#).
- [40] C. Bignamini, B. Grinstein, F. Piccinini, A. Polosa, and C. Sabelli, *Phys.Rev.Lett.* **103**, 162001 (2009), [arXiv:0906.0882 \[hep-ph\]](#); C. Bignamini, B. Grinstein, F. Piccinini, A. Polosa, V. Riquer, *et al.*, *Phys.Lett.* **B684**, 228 (2010), [arXiv:0912.5064 \[hep-ph\]](#); A. Esposito, B. Grinstein, L. Maiani, F. Piccinini, A. Pilloni, A. D. Polosa, and V. Riquer, *Chin.Phys.* **C42**, 114107 (2018), [arXiv:1709.09631 \[hep-ph\]](#).
- [41] L. Liu, K. Orginos, F.-K. Guo, C. Hanhart, and U.-G. Meißner, *Phys.Rev.* **D87**, 014508 (2013), [arXiv:1208.4535 \[hep-lat\]](#).
- [42] R. Casalbuoni, A. Deandrea, N. Di Bartolomeo, R. Gatto, F. Feruglio, *et al.*, *Phys.Rept.* **281**, 145 (1997), [arXiv:hep-ph/9605342 \[hep-ph\]](#); P. Artoisenet and E. Braaten, *Phys.Rev.* **D83**, 014019 (2011), [arXiv:1007.2868 \[hep-ph\]](#).
- [43] C. Meng, H. Han, and K.-T. Chao, *Phys.Rev.* **D96**, 074014 (2013), [arXiv:1304.6710 \[hep-ph\]](#); M. Butenschoen, Z.-G. He, and B. A. Kniehl, *Phys.Rev.* **D88**, 011501 (2013), [arXiv:1303.6524 \[hep-ph\]](#); M. Albaladejo, F.-K. Guo, C. Hanhart, U.-G. Meißner, J. Nieves, A. Nogga, and Z. Yang, *Chin.Phys.* **C41**, 121001 (2017), [arXiv:1709.09101 \[hep-ph\]](#); W. Wang, *Chin.Phys.* **42**, 043103 (2018), [arXiv:1709.10382 \[hep-ph\]](#).
- [44] CMS Collaboration (CMS) (2019), [CMS-PAS-HIN-19-005](#).
- [45] J. Adam *et al.* (ALICE), *Phys.Rev.* **C93**, 024917 (2016), [arXiv:1506.08951 \[nucl-ex\]](#); S. Acharya *et al.* (ALICE), *Phys.Lett.* **B800**, 135043 (2020), [arXiv:1906.03136 \[nucl-ex\]](#).
- [46] H. Zhang, J. Liao, E. Wang, Q. Wang, and H. Xing, [arXiv:2004.00024 \[hep-ph\]](#) (2020); B. Wu, X. Du, M. Sibila, and R. Rapp, [arXiv:2006.09945 \[nucl-th\]](#) (2020).